Chapter

# Ion Beam Experiments to Emulate Nuclear Fusion Environment on Structural Materials at CMAM

*Marcelo Roldán, Patricia Galán, Fernando José Sánchez, Isabel García-Cortés, David Jiménez-Rey and Pilar Fernández*

## Abstract

One of the major problems not only in nuclear fusion but in all the fields that have to face irradiation damage is to predict the microstructural evolution of all the features that are involved in the good response of the material. In the case of nuclear fusion, it is well known that structural materials that will be a fundamental piece in the future reactor must withstand severe neutron irradiation damage, high temperatures, and cyclic stresses which will result in a reduction of the lifetime of the component. For that reason, a big effort is being done for the scientific community in order to understand the complex mechanisms that lie in the relationship between irradiation damage, microstructure, temperature, stresses, etc. However, neutron irradiation brings inherently transmutation and nuclear activation, which makes extremely hard to study those samples. Therefore, the scientific community is using since long time ago ion beam facilities to emulate the neutron damage, without the worst inconvenience. In this chapter, the authors described briefly the facility located at Centro de MicroAnálisis de Materiales (CMAM), Madrid, and presented afterward some examples of experiments that Spanish Nuclear Fusion Laboratory at CIEMAT has been carrying out related to this matter.

**Keywords:** structural materials, nuclear fusion, ion beam irradiation, irradiation damage, modeling

## 1. Introduction

Structural materials for nuclear fusion applications will have to withstand a very hard environment in the future reactor. Very energetic neutrons which will produce displacement cascades, transmutation into light atoms, nuclear activation and nuclear heating will be produced during operation. These neutron reactions, along with stresses produced by the reactor weight itself, and cyclic loads due to thermal and electromagnetic stresses draw a very harsh panorama for these materials [1–4].

Neutrons from nuclear fusion reaction induce elastic and inelastic nuclear reactions. The very first atoms from the matrix displaced by the incident neutron are denominated Primary Knock-on Atoms (PKA) spectrum, and this PKA spectrum is generated by both elastic and inelastic reactions. Generally speaking, depending on the isotope considered, the larger contribution to the total displacement is due to the elastic reactions (90%). However, atoms initially displaced for their lattice site

by neutrons (PKA spectrum) will induce elastic reactions, which produce additional displacement damage (displacement cascades) because they eventually will produce large collision cascades, since the secondary atom impacted by the PKA has enough energy to move a third one and so on.

Therefore, this PKA spectrum will be responsible to deposit the displacement damage in the material. On the other hand, if the neutron produced an inelastic reaction, an induced transmutation by neutron collision will be produced, generating light atoms as helium and hydrogen until hundreds of atomic parts per million (appm) in the whole life service of the reactor along with PKAs depending on the energy deposited [5].

Regarding helium atoms, one of the main issues in terms of structural material degradation is the nucleation and growth of He bubbles at grain boundaries which would produce a reduction of service lifetime. This degradation comes due to helium atoms produced by transmutation reaction of Fe; around 4 MeV of neutron energy may produce the following reaction generating alpha particles 56Fe (n.a) 53Cr [6]. It is well known that the combination between helium atoms and vacancies is very energetically favorable, so it will form eventually He bubbles. For that reason a deeper understanding of the effect of those bubbles in the evolution of microstructure and further degradation of mechanical properties are critical. However, several parameters have to be controlled and studied to determine properly the evolution of He bubbles during irradiation such as temperature, He production rate, displacement rate, and dose (accumulation of He).

Candidate materials for being used as structural materials are reduced activation ferritic martensitic (RAFM) steels, since they show a high resistance to irradiation damage, higher thermal conductivity, good corrosion resistance, and good liquid metal compatibility than austenitic steels. Several studies have shown that grain boundaries or phase boundaries may also act as sinks for radiation-induced point defects and the cluster formed during irradiation [7].

On the other hand, collision cascades known as accumulation of atoms displaced will form a complex form of Frenkel pair defects such as interstitial clusters which may turn into large dislocation loops or vacancy-type voids. Those irradiation-induced defects act as barriers to the dislocation movement, so they produce a significant hardening and hence a ductility reduction.

Neutron irradiation is not the most used technique to irradiate materials since the nuclear activation of the specimens makes necessary to have available hot cells to characterize the samples. On the other hand, nowadays there is no facility to emulate neutron fusion environment; for that reason ion beam irradiations are used to emulate neutron irradiation, of course, having into consideration the main differences such as shallow depth of irradiated material, elevated dose rate, and, clearly, not transmutation.

Current neutron sources with an energy spectrum typical of fusion reactions (14 MeV neutrons) are far from the fluence expected in a fusion reactor, and they are only useful for a few cases involving functional materials not exposed to high radiation doses [8, 9]. Therefore, a common approximation to test fusion materials consists of using ion irradiation to emulate the effects of neutron irradiation [10]. Ion irradiation can yield higher damage rates generating negligible activation levels in the irradiated samples at a reduced cost than other approximations to the problem like fission reactor irradiations. These elevated dose rates are very interesting to obtain samples submitted to an accelerated damage aging that would take several years to be achieved by fission irradiation. It is necessary to consider, however, that these accelerated tests may be driven by aging mechanisms very different from the real processes taking place under the low damage rate produced by real fusion conditions.

Another important difference that must be considered is the low ion penetration in the material (typically several microns for heavy ion energy in the range of 1–20 MeV) compared to the tenths of centimeters that a neutron can travel before interacting with a material nucleus. Since the particle accelerators have a fixed energy, a selective filter or energy degrader system is required to obtain an almost uniform spectrum of beam energies to allow a particle implantation in the most controlled possible way. The thickness of the filter determines the final energy of the beam, so to obtain a certain energy spectrum, it has been thought of a multifilter revolver-type system, consisting of a design in the form of a rotating daisy, with peripheral aluminum foils of different thicknesses in order to achieve different mitigations of the beam energy [11].

As stated before, to date, most of the studies on these structural materials have been focused on material behavior as a function of different parameters as irradiation dose, particle energy, and irradiation temperature, among others [12]. However, next-step fusion devices, such as the International Thermonuclear Experimental Reactor (ITER) [13] and demonstration power plant (DEMO) [2, 14, 15], are magnetically confined devices, and the performance of the materials under reactor conditions when high magnetic fields are present is still unexplored. Besides, theoretical predictions suggest that magnetism can be a non-negligible factor in defining the defect properties induced by He irradiation or in determining the atomic distribution in FeCr alloys [16, 17]. Material microstructural properties can be modified by defect propagation due to irradiation. It is considered that such propagation may be affected by external magnetic fields, as recently pointed in Ref. [18]. For this reason, more detailed experimental knowledge of structural materials is sought, in particular with regard to mobility and clustering, as well as helium and hydrogen accumulation in reactor conditions. Thus, expanded experimental knowledge of structural material response to irradiation under magnetic fields has become critical.

In this chapter, the development of a new sample holder located at a vacuum chamber of standard (STD) irradiation line at CMAM is presented. Preliminary results have been obtained in this system for a series of FeCr alloy (10–15% Cr), alloy specimens irradiated with 1 MeV $Fe^{+}$ ions under the effect of the magnetic field produced by a permanent magnet (0.5 T) at STD irradiation line at CMAM.

As sometimes, experiments are costly even with ion beams and are not always available; modeling is one of the key tools to predict long-term defect evolution. However, irradiation damage predictive simulation is still under development and needs many experimental results as inputs to validate their simulations. So, sometimes, irradiation experiments are headed not only to study the degradation of complex microstructure materials such as RAFM candidates but to obtain results of irradiating very simple and pure such as very high pure iron, iron chromium model alloys in order to study the effect of certain alloying elements on irradiation defects evolution.

Electrostatic accelerators over the world present a variety of shapes and sizes and can be classified attending to different factors. The fundamental features that characterize a DC accelerator are mainly three: the type of particle that can accelerate, the beam current and the maximum kinetic energy achievable. These defining parameters determine the subsequent research field of application.

## 2. Accelerator description

In this section, we describe the fundamentals of a 5 MV Tandetron delivered by high-voltage engineering (HVE) for ion beam analysis (IBA) and ion beam modification of materials (IBMM) at operation in CMAM in the Universidad Autónoma de Madrid (Spain) [19]. In **Figure 1** it is possible to observe (a) plan view of the

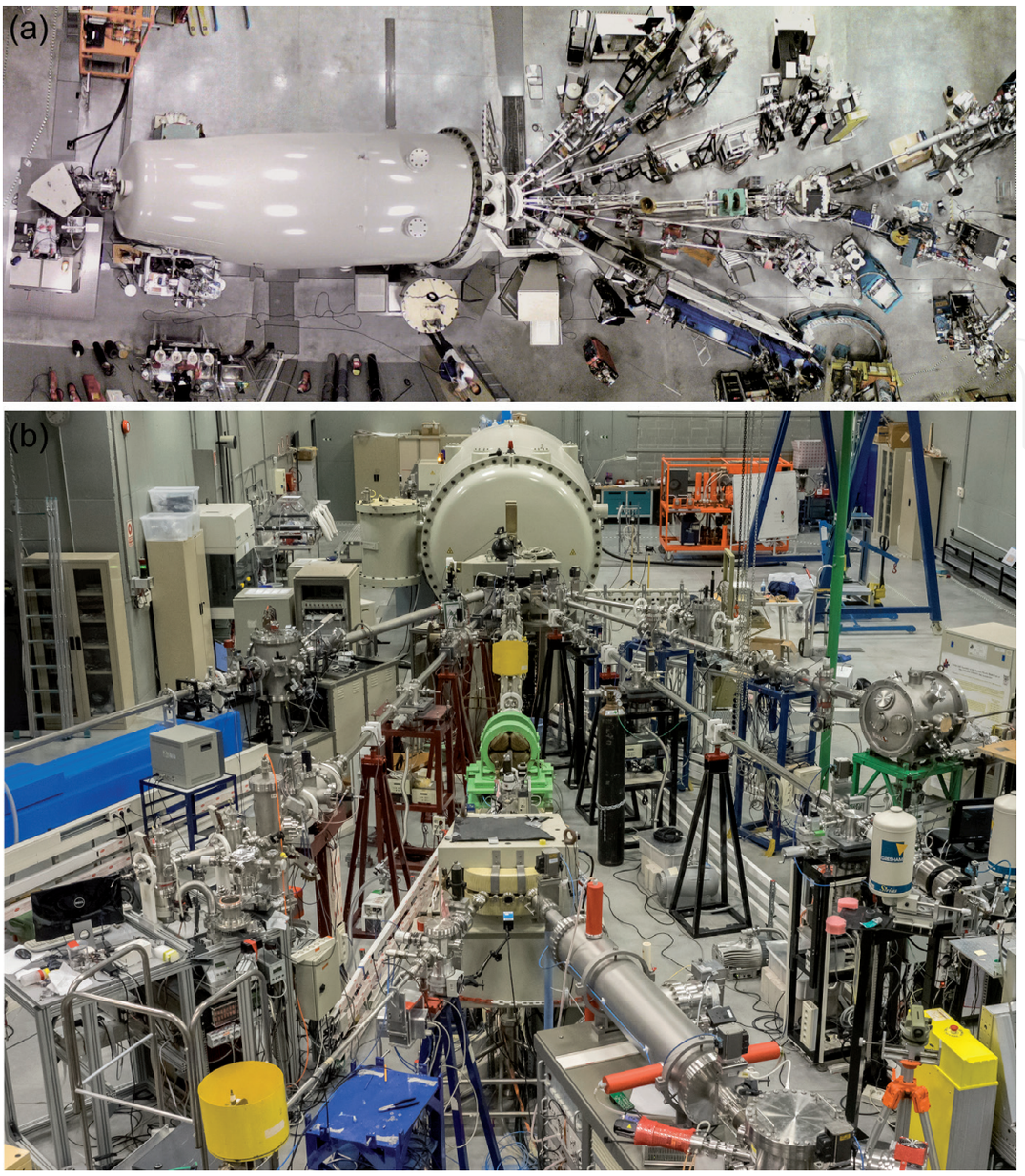


**Figure 1.**
*(a) Plan view of the tank and the lines of CMAM accelerator and (b) detail of the accelerator lines (courtesy of Jorge Álvarez Echenique, CMAM).*

mentioned accelerator and (b) all the lines which are nowadays working. This kind of facility is also of great interest to investigate fusion-induced material damages by creating a controlled environment to simulate these effects.

The Tandetron ion accelerator is a tandem type that counts with a Cockroft-Walton high-voltage generator system that will be presented briefly in the following paragraphs, describing sources for ion beam generation, beam acceleration, and two of the beamlines available used for experiments for nuclear fusion.

## 2.1 Ion beam production

The first step for IBA or IBMM experiments is to generate the beam, i.e., to produce ions from neutral matter, extract them, and focus the beam. Since the selected ion and the current are a function of the experimental needs, the source constraints are of critical importance. CMAM facility is provided with two sources: a plasma source for gaseous substances and a sputtering source to obtain practically any element of the periodic table from a solid target.

The range of current that can be obtained from the source varies from a few nA to tens of μA, depending on the source and the ion. As will be presented later, the tandem configuration requires the production of negative ions, which are more difficult to obtain than positive ones. It is much easier to rip off electrons from an atom than to add them on. It is not even possible to obtain negative ions from all elements, as is the case of nitrogen, so unstable that in practice cannot be produced [23].

This section addresses basic ideas of two specific kinds of ion sources, duoplasmatron and negative sputtering source.

### *2.1.1 Negative sputtering source (model HVE-860C)*

In this configuration, negative ions are effectively produced from a solid target which contains the desired beam material inside a cylindrical refrigerated copper cathode, the sputter target holder. A cesium reservoir is heated providing vapor to the main cavity of the source. The neutral flux of Cs has two functions: on the one hand, the cesium condensates over the target surface, and, on the other hand, a fraction of the Cs atoms in the gas becomes positively ionized by contact with a heated ionizer surface. The ionizer is kept at positive voltage with respect to the cathode so that positive Cs ions bombard the target producing the ejection of sputtered atoms that pass through the optimally cesiated surface with a low work function [20, 21]. By this surface effect method that involves cesium as a great electron donor, sputtered atoms from the target become negative (secondary negative ions). Those ions are repelled from the cathode to the extraction section of the source and focus into a negative beam. Beam currents of 2–40 μA are achieved, depending on the species. Elements with negative electronic affinity, such as nitrogen, can be extracted from the source in the form of a molecular beam (e.g. $NH^-$) and broken into its components at a later stage. Any element of the periodic table from hydrogen to uranium can be delivered, with the important exception of helium.

### *2.1.2 Duoplasmatron source (model HVE-358)*

The duoplasmatron source permits two modes of operation, positive and negative ion beam extraction from a gas (typically $H_2$ or He). Positive operation is required for helium atoms because being a noble gas is not possible to efficiently obtain negative helium ions directly from the source. After positive extraction, He+ ions pass through a charge-exchange cell filled with lithium vapor where the final negative beam emerges for further acceleration. Only about 1% of the He+ ions coming from the source turn negative, a fact that limits the maximum achievable current to a few μA versus tens of μA obtained when working in negative operation.

The working principle of ion generation consists of a two-stage discharge where the gas is leaked into the source and the molecules are ionized. The first discharge is produced by means of thermo-ionic emission from a hot filament, between the filament (cathode) and the intermediate electrode (IE). A strong confining magnetic field guides the electrons through an aperture to the second discharge region between the intermediate electrode and the anode [22]. The magnetic field and the geometry of the IE are specially configured to enhance plasma density and high ionization degree. Finally, regarding the extraction direction, just comment that the ions are axially extracted from the plasma.

### *2.1.3 Injector system*

The ions in the beam exiting the source are shaped, focused, and led to the entrance of the accelerator, passing through a 90° analyzing magnet that bends the

beam and selects the proper mass of the single negative-charged ions. Mass separation is done by tuning the magnetic induction so that only a given $q/\sqrt{m}$ ratio is transmitted through the entrance and exit collimators. This is necessary because the beam exiting the source contains several species along with the desired one due to imperfect vacuum or impurities in the target. The electromagnet is water-cooled and capable of inflecting all ions in the periodic table, selecting them by momentum per unit charge, i.e., by magnetic rigidity [Eq. (1)] [23]:

$$Br = \frac{p}{q} = \left(\frac{2mE}{q^2}\right)^{1/2} \quad (1)$$

where B is the tunable magnetic induction, m the desired mass of the particle, E its energy, q its charge, and r the radius of curvature of its trajectory, which is determined by the entrance and exit of the magnet.

The guidance and focusing of the beam during its trajectory are achieved by electrostatic and magnetic devices called lenses for the analogy that can be drawn with the effect of thick optical lenses on light. Moreover, electrostatic or magnetic deflectors properly steer the beam into the optical axes of the lenses so that adjusting the lens will alter the focus but not the position of the beam.

### 2.2 Tandem accelerator system

Following the injector system, the beam containing negative ions at a certain kinetic energy defined by the extraction voltages of the sources (tens of kV) goes through the next stage, the accelerator.

A tandem-type accelerator system consists of a two-step acceleration process. The high-voltage terminal electrode is enclosed in the center of a pressure vessel midway between the entrance and the exit of the acceleration tube, both at ground potential. Once injected into the low-energy part of the tube, the ions get attracted toward the positive terminal, increasing their energy in $nV_T$ electronvolts, where $V_T$ is the terminal voltage and n is the charge state, equal to 1. At this point, the beam passes through a region where $N_2$ gas circulates, getting stripped off from one or more electrons, thus inverting their polarity and getting accelerated again to ground along the high-energy tube. The beam is composed now of a distribution of positive charge states n that vary from 1 to Z, Z being the atomic number of the atom. This second step leads to an energy gain of $nV_T$ electronvolts that depends on the specific charge state of each ion [24].

The extra energy obtained by inverting the polarity is the primary benefit of tandem-type accelerators over single-ended ones and the reason why negative ion sources are required. Additionally, this system allows the sources to be outside the tank, a fact that implies easier maintenance and simpler operation of the sources. On the contrary, the charge-exchange process results in a reduction of beam intensity, especially for heavy ions, being the transmission up to 50%. However, for IBA analysis and many material experiments, these currents are adequate.

The total kinetic energy achieved at the end of the accelerator tube is given in electronvolts [Eq. (2)]:

$$E = E_{ext} + (1 + n)\, V_T \quad (2)$$

where $E_{ext}$ is the extraction energy and $V_T$ is the positive terminal voltage, with a maximum nominal value of 5 MV.

Effective focusing of the beam waist at stripper canal is achieved by optically matching the injector part to the accelerator with a pre-acceleration electrode called Q-snout.

### *2.2.1 High-voltage power generator: Cockroft-Walton*

The engineering challenge of electrostatic accelerators relies on how to produce high voltages, which main limitation is the breakdown due to insulation problems.

As was previously described, the positive high-voltage terminal is located at the center of the tube. But in electrostatic accelerators, the high voltage is gradually distributed among multiple equipotential tubes with a slightly increased value, so that the ions feel a stepwise acceleration in the insulated gaps between each segment. That keeps a reduced value of the local electric field.

The accelerator at CMAM produces the terminal voltage by means of a Cockroft-Walton (C-W) generator system, a design based on a cascade-type voltage multiplier circuit that was implemented for the first time in a DC accelerator in 1932 by J. D. Cockcroft and E. T. Walton [23] at the Cavendish Laboratory in England. It consists of a circuit feed by radio-frequency (RF) voltage power that supplies a higher DC voltage level. It is constituted by an assembly of repeated units of capacitors and rectifier diodes that double the voltage amplitude with each additional block. A final voltage of 2 nV is obtained, where n is the number of repeated blocks, 50 in the case of CMAM Tandetron [24], and $V_o$ is the amplitude of the AC voltage. A simplified scheme of the multiplier circuit invented by Greinacher [25, 26] in 1921 is shown in **Figure 2**.

The hole voltage multiplier structure is placed around the evacuated acceleration tube in a coaxial configuration. High vacuum is required inside the tube to minimize unwanted secondary electron production by collisions of the ions with atoms of the residual gas. Furthermore, small magnets are placed to suppress these backstreaming electrons before they get accelerated generating hard X-rays. The electrodes are parallel fed with the increasing potential by resistive grading, and thus the voltage is smoothly distributed from terminal to ground. All the assembly is enclosed inside a pressurized tank filled with insulating sulfur hexafluoride gas (SF6) to prevent electrical breakdown, and every component is specifically designed to reduce local electric stress to avoid corona and sparking [22].

The advantage of C-W generator system relies on being entirely based on a solid-state circuit. The absence of moving parts, the high RF driving frequency (~38 kHz), a special RC filtering, and the feedback circuits that monitor the terminal voltage through a generating voltmeter (GMV) provide a remarkable terminal voltage stability and low terminal voltage ripple (less than 50 V at 5 MV). As a result, a superior beam energy resolution is achieved.

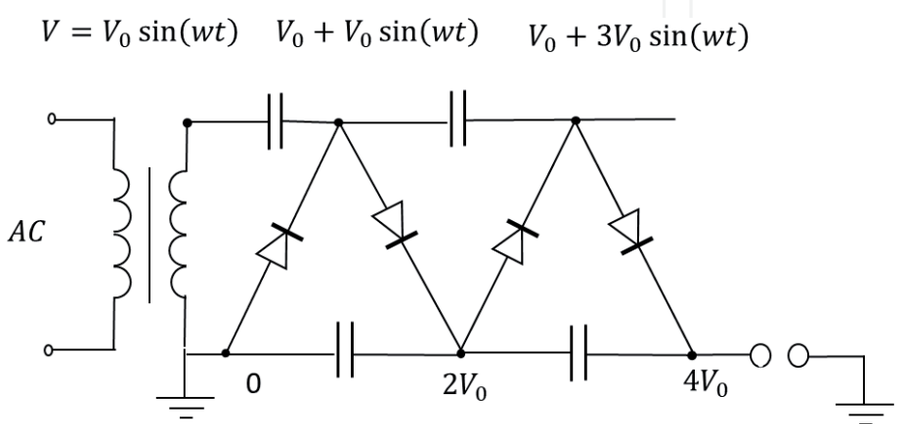


**Figure 2.**
*Simplified scheme of the Cockroft-Walton generator. The voltage across each stage of the cascade is equal to twice the peak input voltage in a half-wave rectifier.*

## 2.3 Beamlines

After acceleration, the beam is finally focused by an electrostatic quadrupole triplet lens. The first and third quadrupoles focus in the vertical direction (Y-axis) and defocus horizontally (X-axis), while the quadrupole in the middle makes the opposite.

A second magnet with seven exit ports at different angles steers the beam to direct it through an evacuated pipe to the selected experimental station. Since the beam is composed of a distribution of charge states n, the switching magnet has the additional important role of discriminating a certain charge state in order to establish well-defined beam energy.

CMAM counts with six operative beamlines devoted to different research fields: standard multipurpose beamline, internal μ-beam line, ERDA-ToF line, implantation beamline, external μ-beam line, and nuclear physics beamline.

The essential features of two of the routinely used beamlines for experiments for structural materials for nuclear fusion applications at CMAM accelerator are outlined below.

### *2.3.1 Multipurpose or standard beamline*

This line is attached to the 30° port of the switching magnet and is the one that was initially installed and tested by HVE. The experimental chamber is placed 3.5 meters away from the magnet, not needing additional focusing. A set of two slits separated 2 m from each other are used to control the size and divergence of the beam, and the current can be measured with a Faraday cup located immediately before reaching the chamber [27].

The standard line is mainly devoted to Rutherford backscattering spectrometry (RBS) and elastic recoil detection, but several ports are available to position additional setup. The entire structure is kept under high-vacuum conditions by means of a turbomolecular pump assisted by a rotary pump.

A fixed Si barrier particle detector is located at 170° with respect to the incident beam, while another movable detector can be positioned at any angle, counting with a carousel with different foils and slits that can be positioned in front of the movable detector. Also, an SDD detector for simultaneous particle-induced X-ray emission (PIXE) performance is implemented.

The sample holder is mounted on a three-axis goniometer and a vertical platform that permits to position the samples and to orient them with respect to the incident beam, so random and channeling experiments can be performed. The sample holder is electrically isolated; it can be biased at +180 V to suppress the effect of secondary electron emission, and the total dose or fluence can be monitored during irradiation by means of a current meter and integrator from HVE [28].

### *2.3.2 Implantation beamline*

The implantation CMAM beamline is at −20° with respect to the accelerator axis, 6 meters after a second switching magnet located at 0° line.

Ion beam modification of materials (IBMM) is the main research field carried out in this line, given that high electronic stopping powers and penetrations of several microns are achievable. Irradiation with ions from H to Pb at maximum terminal voltage can be performed selecting their more prolific charge state, i.e., irradiating with the highest current beam attainable. That allows heavy ion irradiations within the range of 2–50 MeV and currents up to a few μA, depending on the ion. The experimentation chamber is electrically isolated and designed for ultrahigh

vacuum (UHV). Samples' temperature can be modified with a cryostat/furnace designed at CMAM within a range of −180–600°C and precisely controlled during irradiations with a system of thermocouples located at the sample holder and a thermographic camera.

An important feature of this beamline is the capability of performing irradiations over large areas, up to 10 × 10 $cm^2$ on target. An electrostatic beam sweeper of HVE is installed, which deflects the beam a maximum of 9 mm both in vertical and horizontal directions. The beam sweeper permits to scan the irradiation area at 2 and 31 kHz rates in X and Y directions, controlling the beam offset position and scan amplitude. In that way, homogeneous quasi-static beam areas are delivered, as observed in several images below (**Figures 8, 9, 11**, and **13**).

The irradiation fluence is calculated by measuring the beam current with a Faraday cup in the line and the irradiation area with the aid of a scintillator.

#### *2.3.2.1 Beam energy degrader prototype for H, He, and Fe irradiation with a broad profile*

As it was described above, many applications of particle accelerators require varying the beam energy in an experimental beamline without changing accelerator settings. A multifoil (variable thickness) beam energy degrader provides a fast, reliable, and reproducible way of setting the beam energy, obtaining a uniform damage and implantation profile for both, heavy and light ions. The prototype installed at the implantation line of the CMAM has a disc with a diameter of 120 mm (**Figure 3**), which rotates at a thousand revolutions per minute to avoid foil melting under high-current beam irradiation [27]. On the outside the disc has nine aluminum foils of different thicknesses to achieve an energy sweep from maximum energy absorption (thicker foils) and minimum energy of ions to minimum energy absorption of the primary ion beam (thinner foils). The tenth window is free to let the ion beam pass without any energy mitigation. The aluminum foil thicknesses chosen for this prototype were 6–50 microns for H and He ions and 0.8–4 microns for heavier ions like Fe.

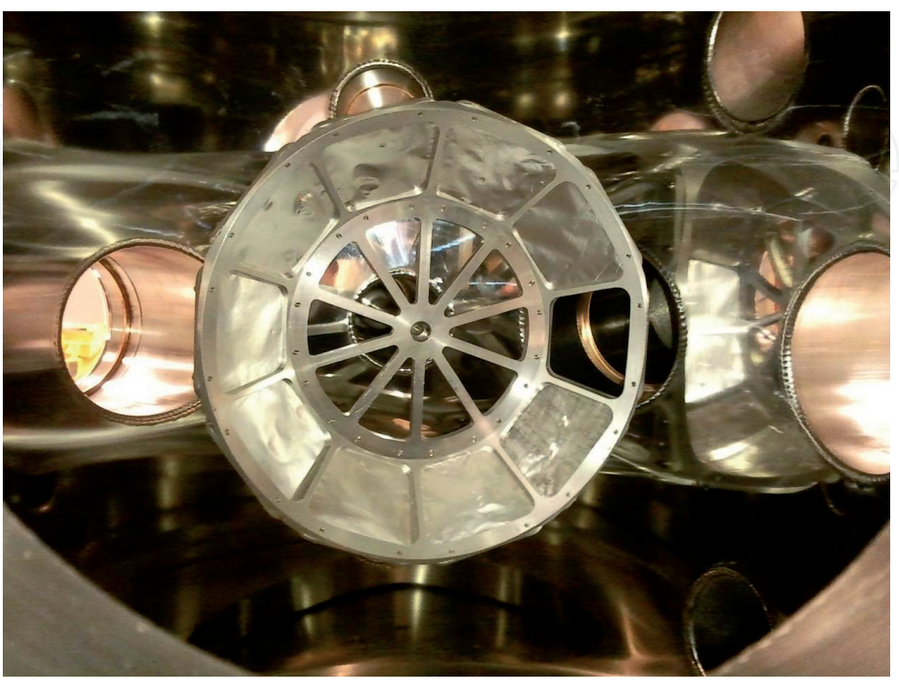

**Figure 3.**
*Umbrella shaped wheel of the beam energy degrader prototype.*

### 2.3.2.2 Motorized sample holder for operation at high temperatures

A water-cooled motorized ferrofluid feedthrough has been chosen with its rotation controller for installation in the specific irradiation chamber of the beam degrader. The controller is able to maintain constant rotation at 1000 rpm and to stop the wheel in the open-blade position to avoid foil damage. The steel vacuum chamber has been designed and manufactured to house properly the degrader wheel, the sample holder itself, and its diagnostics (**Figure 4a**). The necessary set of vacuum pumps and gauges for the degrader chamber has been also installed in the line. Proper butterfly and venting valves were also installed in the vacuum chamber to avoid foil damage during the first stages of chamber air evacuation and venting.

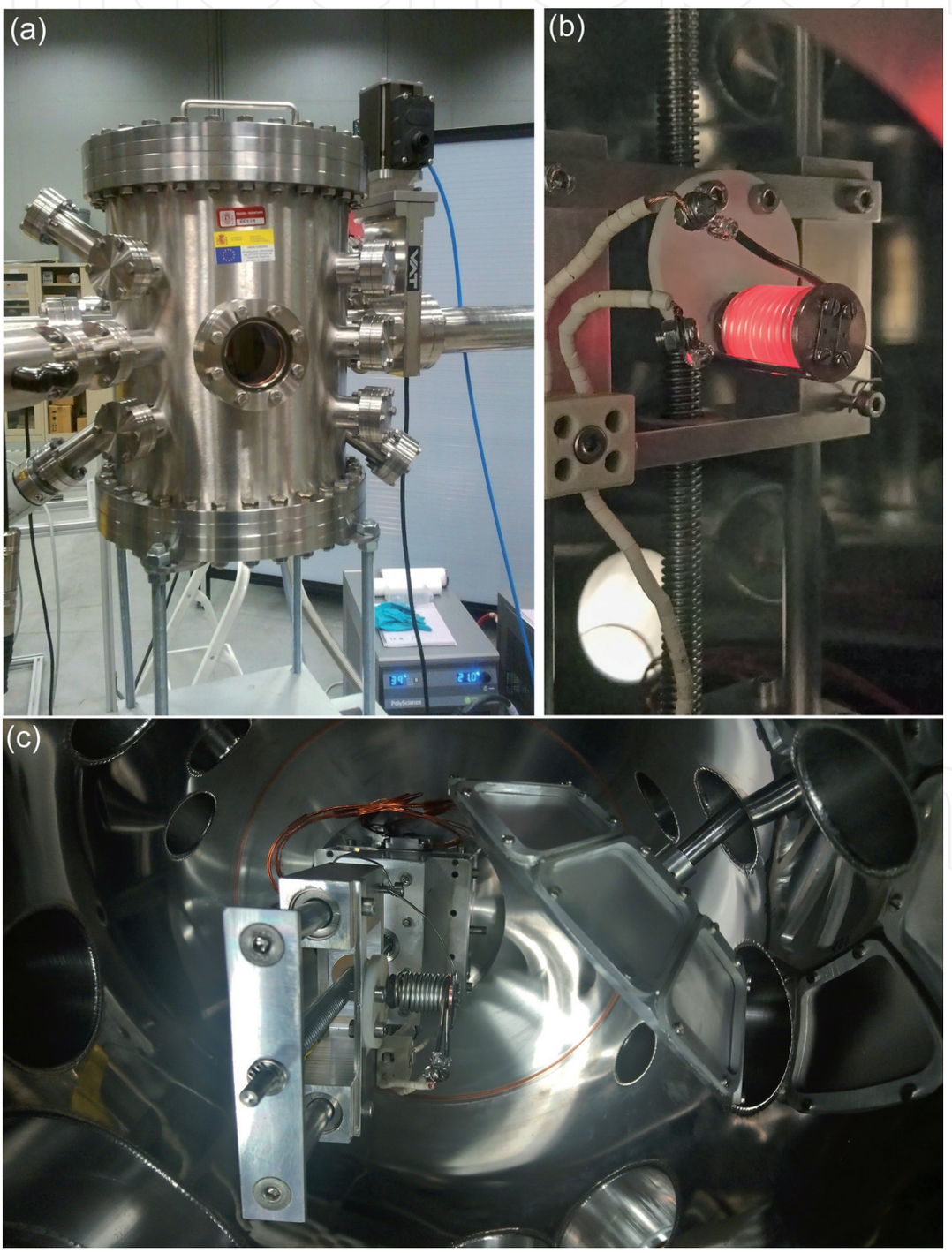


**Figure 4.**
*(a) Vacuum chamber, (b) sample holder oven operating in vacuum at 450°C and (c) vacuum chamber inner view with the degrader wheel and powered sample holder.*

The vacuum chamber includes a sample holder with an oven specially designed to operate at controlled temperature in the range between room temperature (RT) and 600°C (**Figure 4b**) and also it is equipped with an XYZ motorized sample holder for multi-sample experiments (**Figure 4c**).

Several irradiation experiments have been performed using the beam energy degrader. Cu, Fe, and steel samples have been irradiated with H and He ions (current ~ 1 μA) with an energy of 2.25 and 9 MeV, respectively, obtaining implantation profiles with good uniformity from the surface up to 22 μm depth for both ions. This is especially interesting as it is therefore possible to implant both chemical species in the same sample volume. **Figure 5a** shows a SEM cross section of EUROFER97 steel sample implanted with 9 MeV He through a beam degrader with aluminum foils with a thickness from 6 to 50 μm. The implanted sample was etched with Marble's reagent ($CuSO_4$ hydrochloric acid and water) to exhibit the fringes of implanted He. The simulated profile calculated by stopping and range of ions in matter (SRIM) showed great similarities with the real one. Some other experiments have been developed with thinner aluminum foils (0.8–3 μm) and Fe ions with different energies on Fe samples. **Figure 5b** presents the SRIM calculation of the implantation profile of 6 MeV Fe ions on a Fe sample with an average current of 200 nA of $Fe^{2+}$ ions using the degrader device.

Consecutive triple irradiation (Fe, He, H) at temperatures of interest for fusion research (350–550°C) is also available with the experimental setup described in this section, which may be a way to get the nuclear fusion condition with only one accelerator instead of having three of them [29, 30]. To emulate the effects of neutron irradiation, it is therefore possible to irradiate an Fe or steel sample with 20 MeV $Fe^{4+}$ ions with the degrader wheel stopped at the open window (no energy reduction) to obtain a region damaged by Fe ions from the surface up to 2 μm (most Fe ions will stop in the 2–3 μm range generating too many interstitials for a realistic analysis). After that an irradiation with $H^+$ or $He^+$ ions can take place with the degrader wheel spinning with the thinnest foils mounted (0.8–6 μm) and an energy of 1 MeV ($H^+$) and 2 MeV ($He^+$). This procedure would allow to obtain a damaged region uniformly implanted with H and/or He.

### *2.3.2.3 Mini-tensile machine for straining samples under irradiation*

The new vacuum chamber and the beam energy degrader mounted on the implantation line of CMAM irradiation facility also allow the implementation

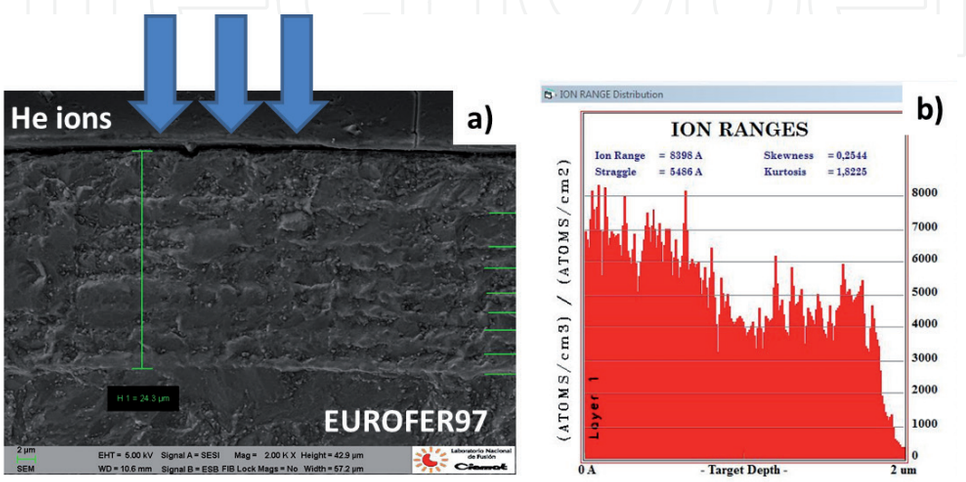


**Figure 5.**
*(a) SEM cross section view of the 9 MeV He irradiation profile on EUROFER97 steel with SRIM simulation and (b) SRIM implantation profile of 6 MeV Fe ions on Fe sample using the thin foil (0.8–3 μm) energy degrader.*

of innovative techniques for material research. In this case we have installed a microtensile test module (**Figure 6**) inside the vacuum chamber in order to carry out mechanical strain/stress tests of materials under irradiation or irradiate structural materials (Fe, Cu, steel), while the sample is submitted to a constant stress. The chamber base shown above and holding the XYZ sample holder can be easily changed by a new one with the microtensile module installed and connected with the proper Fischer feedthrough. Especial connectors are also incorporated for temperature measurements (thermocouple and oven) during the tests.

*2.3.2.4 Sample holder dedicated to the irradiation under magnetic field (STD line of CMAM)*

In order to investigate the influence of an external magnetic field on ion-induced damage, a new experimental system has been developed at the STD line of CMAM. It consists on a dedicated custom sample holder with a permanent magnet embedded behind one of the samples (see **Figure 7a**). Here the samples are irradiated in pairs with and without external magnetic field (B = 0.4 T) with field lines oriented normal to the sample surface in order to avoid ion beam spreading. Commissioning of the system was performed by the irradiation of a luminescent material deposited on a metal support plate. In this way, it was observed that the ions impacting on the luminescent material showed good magnetic field uniformity. In addition, the complete system, i.e., the holder, the permanent magnet, and a UHP-Fe test sample, was also tested during 4 h of irradiation by a 2 MeV, 200 nA

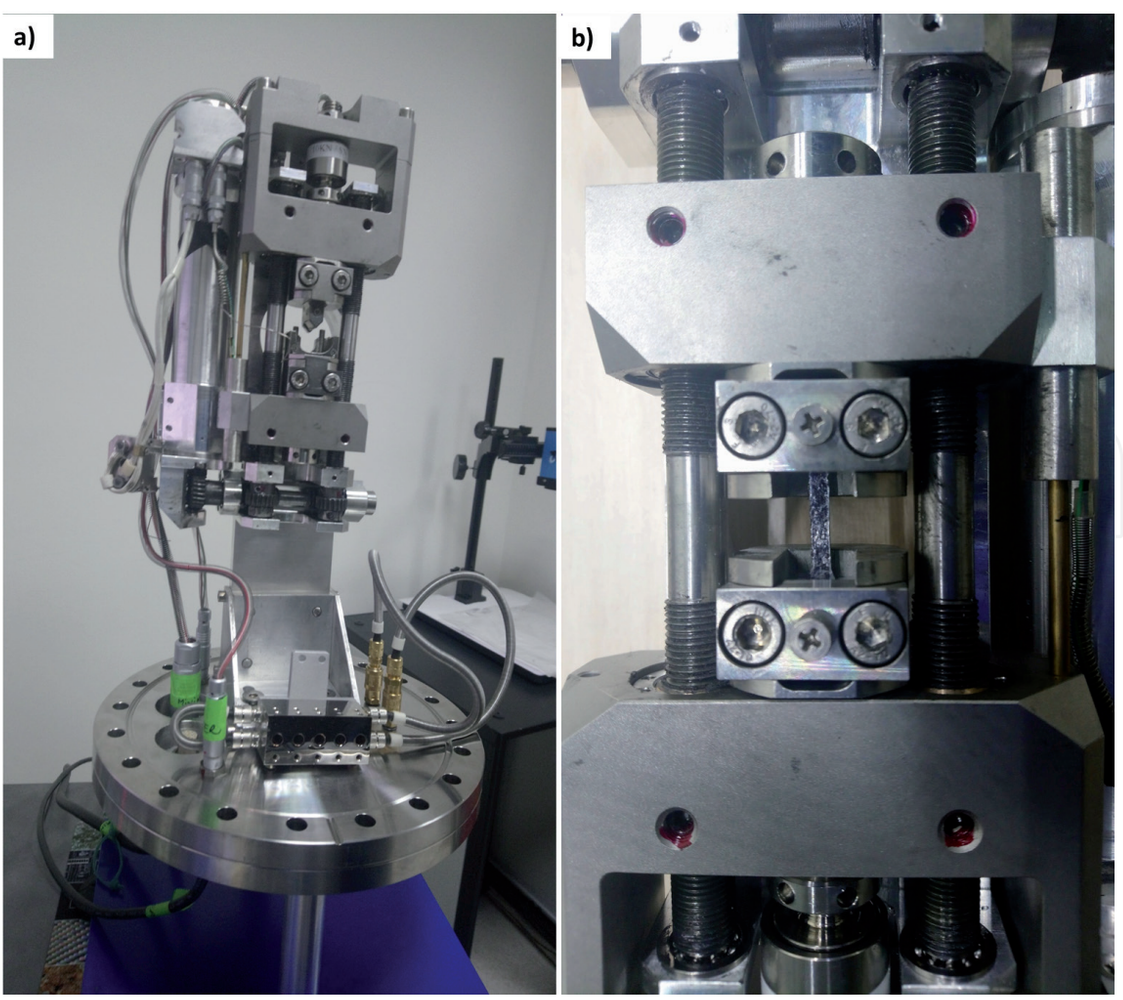


**Figure 6.**
*Microtensile test module mounted in the vacuum chamber base (a) and detail of the test section with a probe (b).*

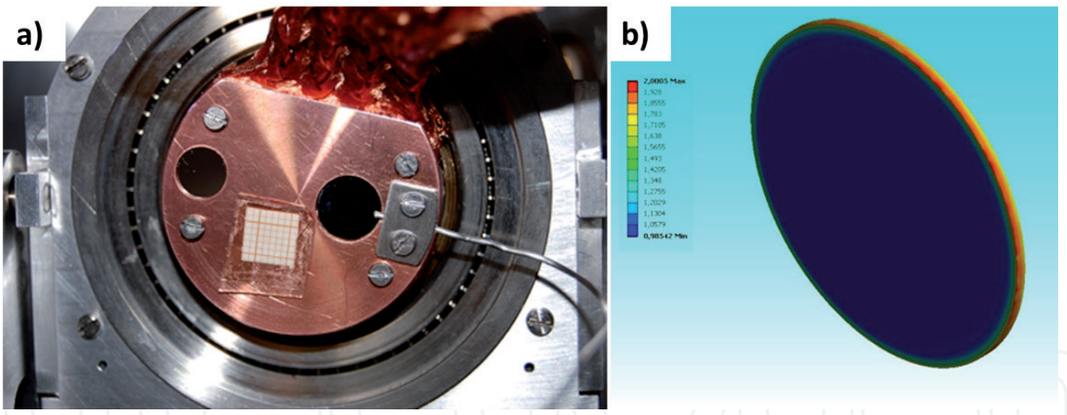


**Figure 7.**
*(a) New sample holder for the irradiation of samples in pairs. It has a permanent magnet behind the right sample. The setup is connected to a LN cooled finger (by a Cu mesh) to achieve low temperature if required. A thermocouple is touching one of the samples for temperature measurements; (b) ANSYS simulation of the magnetic field in the sample near the permanent magnet.*

current H+ beam at a sample temperature of −100°C, with and without magnetic field, getting a good temperature control during irradiation and a same ion beam footprint in sample without B and with B. Although irradiations can generally be performed at low temperature, the analysis is always carried out at RT.

In parallel, prior to starting the experiments, ANSYS simulations were done for Fe90Cr10 slice (1 mm thick) embedded in the center of a long solenoid (giving 1 T in the central column) in order to emulate the effect of B on the surface of the sample. **Figure 7b** shows that although a high concentration of magnetic field lines is observed at the edge, there is good magnetic flux uniformity about the irradiated zone (sample central region), thus validating the experimental setup for use with these samples.

## 3. Experimental results

### 3.1 First results of FeCr alloy damage by ions under magnetic field

A series of experiments have carried out with this sample holder to study the damage in FeCr alloy (14% Cr content) when irradiated at low temperature by heavy ($Fe^+$) and light ($He^+$) ions, single and sequentially, and additionally, the influence of an external magnetic field (B = 0.4 T) was also analyzed [31]. In this context, the influence of B on defects shows small but significant differences in the magnitudes studied here by conversion electron Mössbauer spectroscopy (CEMS) and slow positron annihilation spectroscopy (SPAS). Mössbauer spectra point to less clustering for a sample damaged by He+ (being closer to the as-received sample) than irradiation without B. SPAS points to slightly lower values of vacancy-type defects over a large region when a sample is damaged by self-ions ($Fe^+$, high dose) or by sequential irradiation: $Fe^+$ and $He^+$ (again compared to irradiation without B). SPAS results further support the conclusion that the size or concentration of the vacancy clusters created during the Fe + ion irradiation diminishes in the presence of B.

Also, FeCr alloy (10% Cr) damaged by $Fe^+$ up to 15 dpa (displacement per atom) was analyzed by CEMS and found differences when the magnetic field is present during irradiation [18]. The results indicate that the Cr distribution in the neighborhood of the iron atoms could be changed by the application of an external field.

The detailed studies carried out up to date [18, 31] indicate that an external magnetic field may be an important parameter to take into account in predictive models for Cr behavior in FeCr alloys and especially in fusion conditions where

intense magnetic fields are required for plasma confinement. Experiments with higher B and higher sample temperature are currently in progress in order to elucidate if external magnetic fields are a key parameter in the structural materials damage.

### 3.2 He implantation

Acquiring knowledge concerning fusion transmutation product (He and H) effects on structural materials is difficult to study because of the lack of proper facilities. Using an ion beam accelerator, nuclear fusion-related amount of He was incorporated into the structural material, EUROFER97, using two different ways in terms of beam configuration—defocused beam and raster beam. This is a critical matter to consider because different defect evolution has been detected depending on which method has been taken into consideration to perform the irradiations [32, 33].

#### *3.2.1 Defocused beam*

For this research, a defocused beam was used to implant He into the RAFM steel. This kind of beam configuration has a Gaussian-like profile in terms of ion current with its consequent reduction in density. To establish a valid methodology which allow repetitive and successful experiments, it is necessary to fix some experimental parameters such as ion current, the size of the beam and integration time of the camera that acquires the images from the sample camera because the higher the integration time is, the brighter the image is and the beam size measurements can be wrongly calculated and hence the implanted dose. In order to diminish the numbers of variables to study, irradiation temperature was fixed as room temperature. Hence, the relationship between ion energy, implanted dose, and steel microstructure was studied in terms of radiation defects observed afterward in transmission electron microscopy (TEM).

Regarding the sample holder, as observed in **Figure 8a**, STD line offers a very high flexibility in terms of geometry and size of the samples. Two different squared specimens of steel were attached to the holder along with a wire that was placed underneath to measure the ion current properly and with a current integrator, the implanted dose was calculated accurately. The characteristics of the He ion beam were evaluated by means of ionoluminescence on fused silica, which was used to set up the beam properly: size and stability of the beam prior to irradiation (**Figure 8b**).

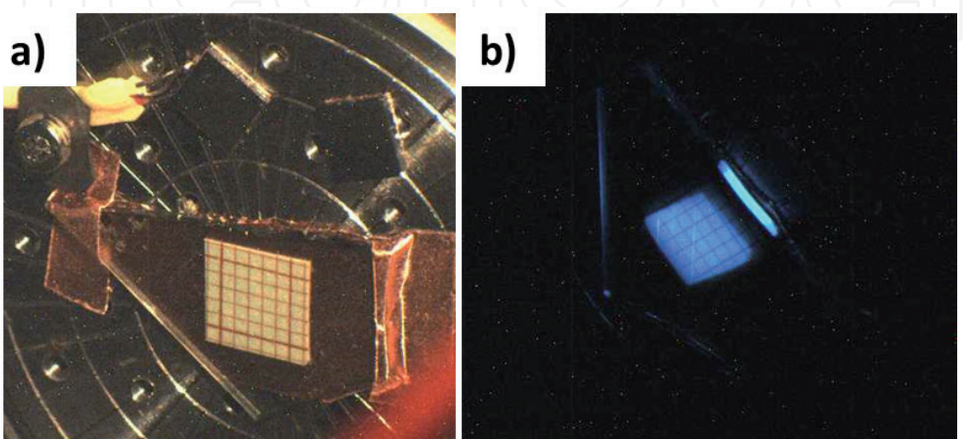


**Figure 8.**
*(a) Irradiation sample holder for implantation beamline. (b) Helium beam irradiating quartz used to measure the quality and size of the beam.*

Before irradiation, simulation code MARLOWE [34, 35] was used to determine the maximum irradiation depth (obtained with 15 MeV in this experiment) and the resultant concentration of He for each energy. It is well known that although the fluence is the same ($1.65 \times 10^{15}$ He ions/cm$^2$) when increasing the ion energy, the peak experiences a broadening, therefore the concentration is the same (integrating the area under the peaks) but the maximum value decreased.

As ion implantation depth is quite shallow in comparison to nuclear irradiation, a stair-like profile of He concentration was used, starting for 15 He MeV and ending with 2 MeV, decreasing the energy in steps of 1 MeV. After implantation, samples were cut and polished through its cross section and were etched in diluted Marble as described before. The etching revealed some lines which represented each and one of the He implantation peaks. Afterwards, the microstructure was observed with a scanning electron microscope (SEM) in order to measure the depth and eventually compare with the simulated position of the stopping peaks for all the implanted energies. The result was that the simulation (**Figure 9a**) and the experiment (**Figure 9b**) matched completely [36]. In addition, it is possible to observe a clear difference with **Figure 5**, where the lines are more diffuse because of the use of a degrader; however, in this experiment, the irradiation peaks are very clear to identify.

### *3.2.2 Raster beam*

The other possibility to perform He irradiation by means of ion beams is using a raster beam. In this case, the beam swept a certain area with a very high frequency. **Figure 10** showed a fused silica emitting light because of the He beam. On the image on the left, the beam swept only the x-axis, the image of the center swept only the y-axis, and on the image on the right, the beam scanned both axes covering the whole area.

Regarding beam heating, as the beam is more focused than the over-focused beam, it is possible that the material experiences a heating which is critical to be measured since the irradiation defects are very temperature sensitive.

A thermographic camera was used to control the aforementioned heating, using as reference a small sample of fused silica because its emissivity and its dependence with temperature are very well known. In **Figure 11**, images taken from the camera are shown after some minutes of irradiation. No important heating was measured, only 15–20°C maximum.

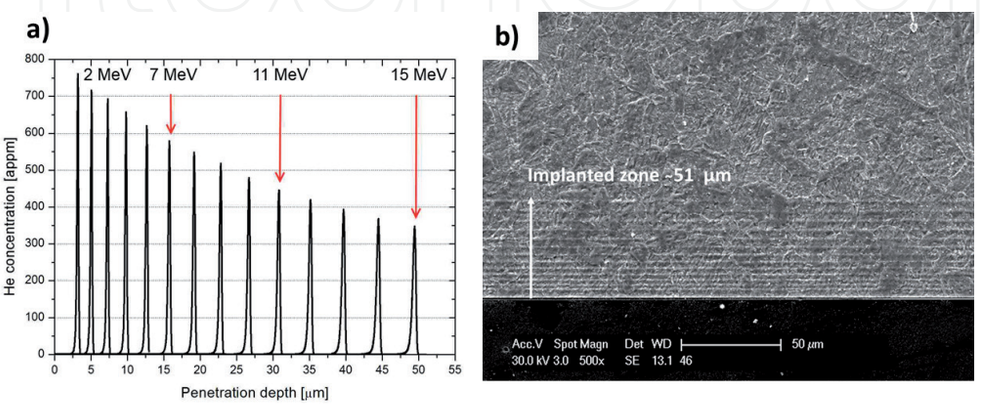


**Figure 9.**
*(a) Depth and helium ion concentration profiles as obtained using MARLOWE code. b) SEM micrograph of EUROFER97 steel implanted with He ions from 15 to 2 MeV, showing the ion stopping region matches with simulation. Published in [36].*

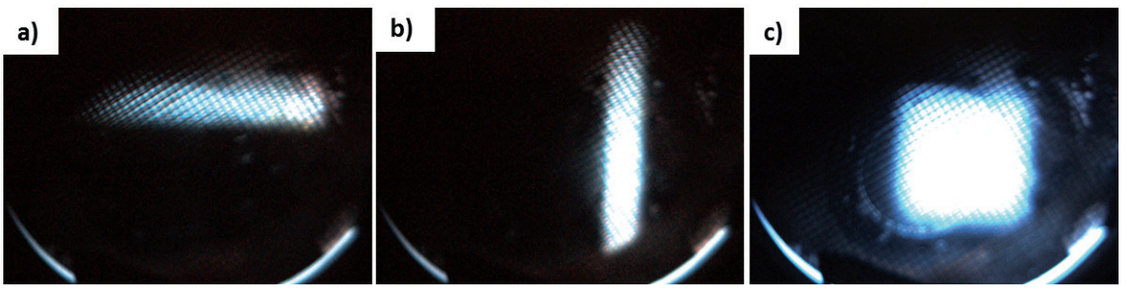


**Figure 10.**
*Ionoluminescence produced by raster beam in different sweeping axes during beam setup. The following images were taken when beam was moving along a) x axis, b) y axis and c) x and y axes together.*

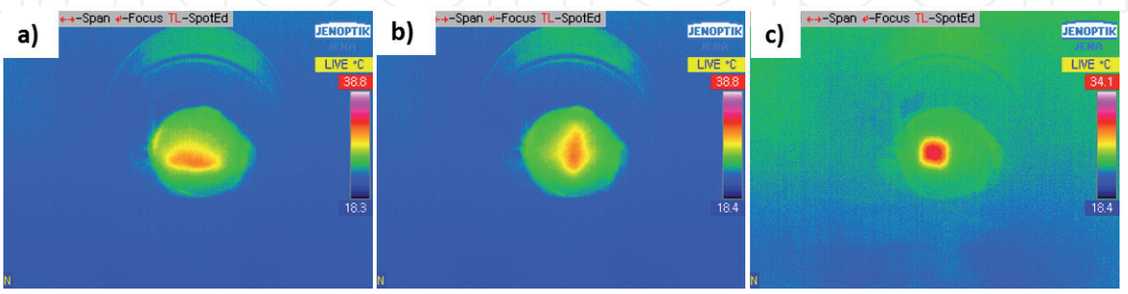


**Figure 11.**
*Thermographic camera images during x-axis (a), y-axis (b), and both axes simultaneously (c) sweeping.*

The sample holder belonging to this line is very flexible, so several specimens can be mounted as observed in **Figure 12a** On the other hand, **Figure 12b** was taken during irradiation. For raster beams, there is no need to measure the beam size before irradiation, since it was determined with the sweeping parameters. However, a way to observe if the beam experienced any kind of sparkling (or any other phenomena which can indicate malfunction) a piece of fused silica was placed along with the specimens in order to observe the beam during irradiation (**Figure 12b**) by means of ionoluminescence as it was done with the defocused beam experiment.

Once the experiment is ended, TEM studies were performed to characterize the defects produced on the steel because of He irradiation. In this case, some TEM discs were prepared by electropolishing, keeping the transparent area within the irradiated area. As mentioned in the introduction, He irradiation may produce

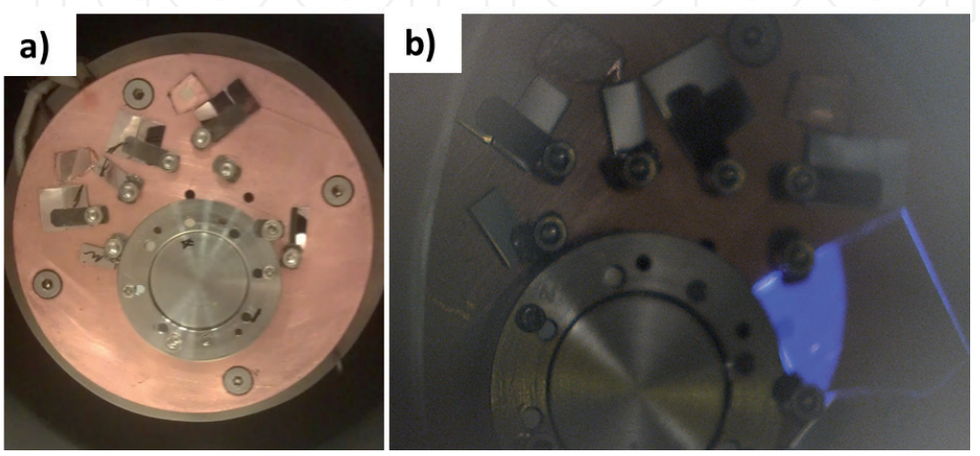


**Figure 12.**
*(a) Sample holder in STD line for raster experiments. (b) Sample holder during irradiation with a circle-shape beam.*

bubbles, and it is well known that a typical way to detect them is through focus serial method, changing the objective length focus distance. When the specimen is found under-focused, the bubbles are observed with white contrast, and on the other hand, when it is over-focused, the bubbles are dark. However, if there are any other microstructural characteristic as secondary phases, grain boundaries, or similar, their contrast remained grayscale-like. In **Figure 13**, three micrographs are presented showing EUROFER97 microstructure with large bubbles within the microstructure (**Figure 13** (a) over-focused, (b) in-focus, and (c) under-focused).

It has been demonstrated that both beam configurations are valid to carry out He implantations. However, more experiments have to be conducted to determine which one is closer to nuclear fusion environment.

### 3.3 Fe implantation

Neutron irradiation produces atomic cascades, as described above, in which the atoms from the matrix moved from their equilibrium positions, generating certain atomic disorder. This disorder stays reflected in dislocation defects as an accumulation of Frenkel pairs. In addition, neutrons also produced transmutation reactions not only generating He and H but radioactive isotopes, thus it would be necessary to keep and test the samples in hot cells. For that reason, a safer and more afforadable way to emulate defects produced by neutrons is to irradiate iron-based alloys such as steels, with Fe ions. Those ions, although they alter a very shallow layer of materials, do not produce transmutation nor modify the chemical composition of the samples so they are called self-ions. There are some examples of irradiations with larger atoms as Xe [37, 38] or Kr [39], although the objective is not the emulation of nuclear fusion environment, since they produce a significant chemical change in the material composition.

Unlike He irradiation, the effect of self-ion irradiation in the microstructure is hard to characterize since the dislocation loops are a very complex features to observe properly and it needs long time and effort, along with a great knowledge of TEM (microscope operation, exquisite sample preparation, and insight of on the theory on irradiation defect generation [40, 41]). In addition, in this field there is a huge gap between simulation models and experiments headed to validate such simulations within the frame of nuclear fusion, so it is an opportunity of irradiating simple alloys which are the base of the complex alloys (i. e. EUROFER97, F82H, ODS steels...). Regarding He bubbles, there is relatively large literature about modeling bubbles in actual steels [42–48], and due to this, the irradiations headed to the understanding of He bubble nucleation and growth carried in this matter are subjected to steels instead of more simple alloys. As in the case of Fe implantation that pure iron is used.

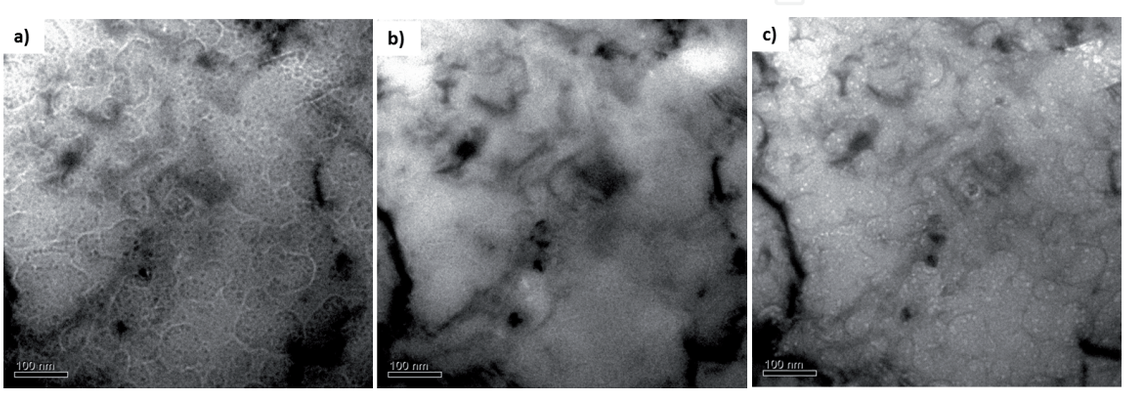


**Figure 13.**
*TEM micrographs showing He bubbles within steel matrix in (a) over-focused (bubbles in black), (b) in-focus (poor contrast), and (c) under-focused (white bubbles).*

For these experiments, the sample holder used was the motorized one which allows high temperature heating as shown in **Figure 14**, This study required a wide range of irradiation temperatures because dislocation loops are very temperature sensitive. The type of beam used was defocused, since the specimens were small (TEM discs), and it was not required to move the beam to cover all the area of interest.

The main goal of this research was to determine if there is a difference in the developing of microstructural irradiation defects because of the temperature and the specimen thickness. The energy used was 20 MeV, and the temperature was 300 and 450°C up to a dose of 5 dpa at the irradiation peak. Several irradiations took place, in order to study two thin foils and two discs (bulk samples) at the two aforementioned temperatures. In **Figure 15**, the damage profile obtained with SRIM is shown. The red curve represented the whole damage peak produced in the bulk samples whose thickness was around 100 μm. On the other hand, the damage generated in the thin foils with a thickness approximately of 100–150 nm fabricated by electropolishing, as the regular TEM disc preparation, is showed with the blue curve, because the ions pass through the thin films. For that reason in bulk specimens, the damage reached the maximum, 5 dpa. However, in thin films the damage is much lower (0.1 dpa), although the ion energy was the same.

Once the irradiations were finished, the samples were studied by TEM. Dislocation loops were found in all the specimens (both bulk and thin foils), but size and distribution were completely different between bulk and thin-film experiments. In the first one, although the damage was much higher, the maximum loop observed was 22 nm, and the distribution was quite heterogeneous, being maximum at the damage peak depth (**Figure 16a** and **b**). Nevertheless, in thin films, in spite of the small amount of thickness and the small amount of damage deposited by self-ions, very large loops were detected, even larger than 500–600 nm distributed homogeneously within the material (**Figure 16c** and **d**). In addition, differences between Burger vectors and population density have been found. Deep characterization is being carried out, but those preliminary results proved that the configuration (accelerator device, irradiation parameters, and sample holder) used in CMAM facility provides the tools required to perform high quality experiments whose results will be of a great support for modeling scientists.

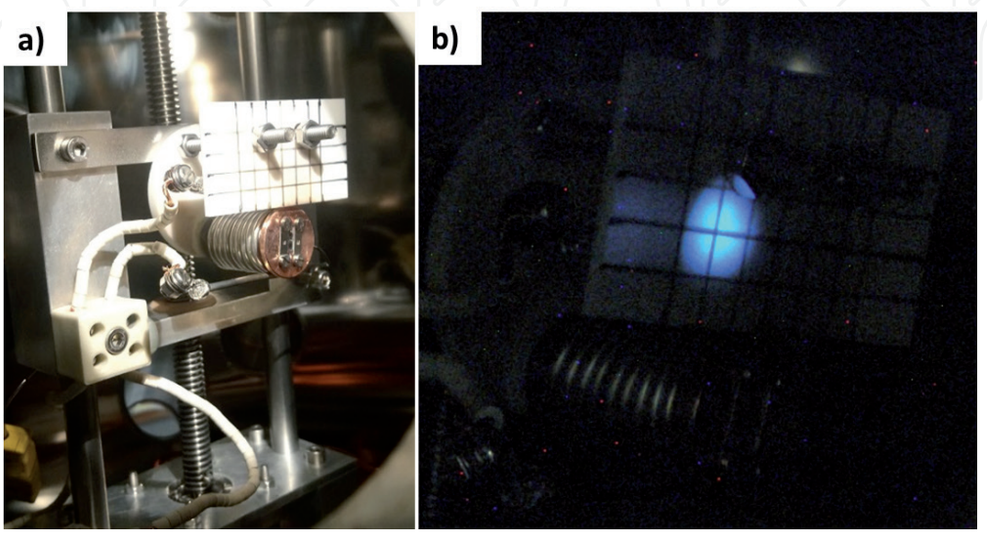


**Figure 14.**
*(a) Motorized sample holder for Fe ion irradiations. (b) Light produced by ionoluminescence because of the irradiation of Fe ions onto MACOR piece.*

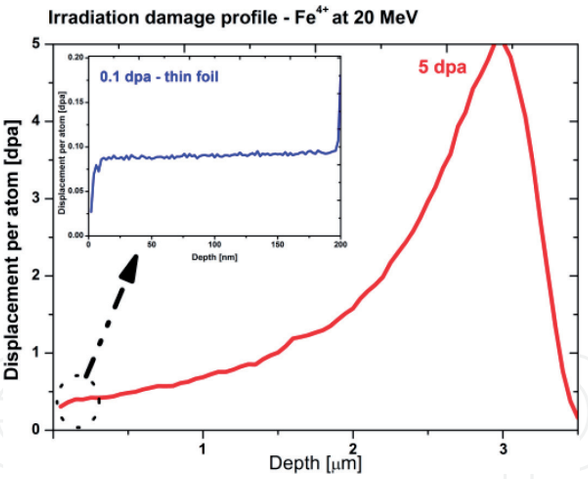


**Figure 15.**
*SRIM profile of bulk irradiation (red curve) and thin-film irradiation (blue curve).*

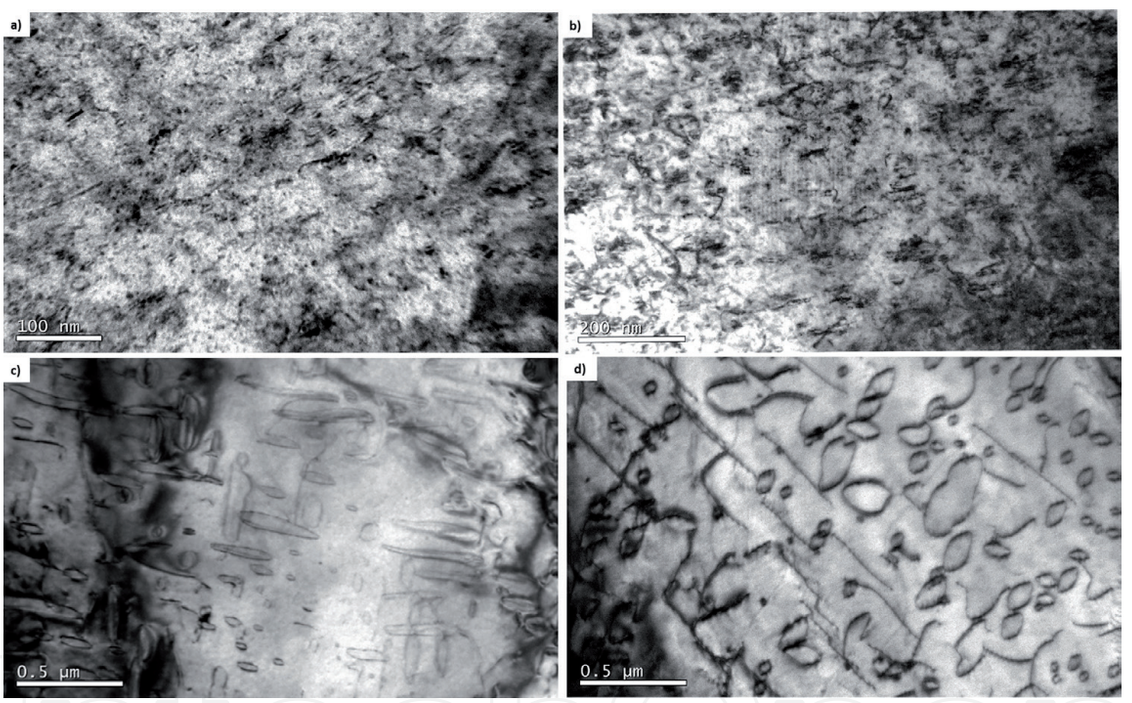


**Figure 16.**
*Dislocation loops found in pure Fe in different experiments in bulk experiments at 5 dpa and (a) 350°C and (b) 450°C and in thin foils at 0.1 dpa at (c) 350°C and (d) 450°C.*

## 4. Conclusions

The importance of ion beam accelerators to perform experiments which gain insight with about the possible synergies between radiation damage, microstructure, strain, and magnetic fields regarding degradation of structural materials for nuclear fusion applications has been presented in this chapter. It is well known that there is a gap between neutron irradiation and ion irradiation, but it is still a very important source of knowledge until the scientific community has the possibility of using a facility which emulates the nuclear fusion environment as DONES [5].

CIEMAT has been carrying out for several years numerous experiments in this field generating vast knowledge about irradiation effects on structural materials, with the help of CMAM facility and its researchers and staff.

Therefore, it has been demonstrated that ion beam accelerators are a fundamental tool to the developing of the future nuclear fusion reactors.

## Acknowledgements

This work has been supported by Ministerio de Ciencia, Innovación y Universidades Projects, ENE2015-70300-C3-1-RE, ENE2016-76755-R, NE2016-76755-R, and MAT2012-384407-C03-01, and TechnoFusion Project (S2013/MAE-2745) of the Comunidad Autónoma Madrid (CAM) and partially by the European Communities within the European Fusion Technology Programme 2014–2018 under agreement No 633053. "The views and opinions expressed herein do not necessarily reflect those of the European Commission."

The authors wanted to thank the National Center for Electron Microscopy (CNME) staff and all the researchers and technician from CIEMAT, specially the researchers working on simulation: F. Mota, C. Ortiz, and F. Jiménez-Piñero. In addition, the authors wanted to extend their gratitude to all CMAM staff for their help, kindness, and contribution with this work. Finally, the authors do not want to miss the opportunity to express the appreciation to High Voltage Engineering Europa B.V. to allow and check this publication.

## Author details

Marcelo Roldán[1*], Patricia Galán[2], Fernando José Sánchez[1], Isabel García-Cortés[1], David Jiménez-Rey[1] and Pilar Fernández[1]

1 CIEMAT, Madrid, Spain

2 CMAM, Madrid, Spain

*Address all correspondence to: marcelo.roldan@ciemat.es

## References

[1] Knaster J, Moeslang A, Muroga T. Materials research for fusion. Nature Physics. 2016;**12**:424-434

[2] Stork D et al. Materials R&D for a timely DEMO: Key findings and recommendations of the EU roadmap materials assessment group. Fusion Engineering and Design. 2014;**89**(7-8):1586-1594

[3] Zinkle SJ, Was GS. Materials challenges in nuclear energy. Acta Materialia. 2013;**61**(3):735-758

[4] Muroga T, Gasparotto M, Zinkle SJ. Overview of materials research for fusion reactors. Fusion Engineering and Design. 2002;**61**(13):13

[5] Mota F et al. Analysis of displacement damage in materials in nuclear fusion facilities (DEMO, IFMIF and TechnoFusion). Fusion Engineering and Design. 2011;**86**(9):2425-2428

[6] Fischer U, Simakov SP, Wilson PPH. Transmutation behaviour of Eurofer under irradiation in the IFMIF test facility and fusion power reactors. Journal of Nuclear Materials. 2004;**329-333**:228-232

[7] Xia LD et al. Radiation damage in helium ion-irradiated reduced activation ferritic/martensitic steel. Nuclear Engineering and Technology. 2018;**50**(1):132-139

[8] Knaster J. An assessment of the available alternatives for fusion relevant neutron sources. Nuclear Fusion. 2018;**58**(9):095001

[9] Zinkle SJ, Möslang A. Evaluation of irradiation facility options for fusion materials research and development. Fusion Engineering and Design. 2013;**88**(6-8):472-482

[10] Was GS. Challenges to the use of ion irradiation for emulating reactor irradiation. Journal of Materials Research. 2015;**30**(09):1158-1182

[11] Chu WT, Ludewigt BA, Renner TR. Instrumentation for treatment of cancer using proton and light-ion beams. Review of Scientific Instruments. 1993;**64**(8):2055-2122

[12] Zinkle SJ. Fusion materials science: Overview of challenges and recent progress. Physics of Plasmas. 2005;**12**(5):058101

[13] Motojima O. The ITER project construction status. Nuclear Fusion. 2015;**55**(10):104023

[14] Yamanishi T et al. Recent technical progress on BA program: DEMO activities and IFMIF/EVEDA. Fusion Engineering and Design. 2016; **109-111**(Part B):1272-1279

[15] Federici G et al. Overview of the design approach and prioritization of R&D activities towards an EU DEMO. Fusion Engineering and Design. 2016;**109-111**(Part B):1464-1474

[16] Seletskaia T et al. Magnetic interactions influence the properties of helium defects in iron. Physical Review Letters. 2005;**94**(4):046403

[17] Malerba L, Caro A, Wallenius J. Multiscale modelling of radiation damage and phase transformations: The challenge of FeCr alloys. Journal of Nuclear Materials. 2008;**382**(2):112-125

[18] Sánchez FJ et al. Influence of an external magnetic field on damage by self-ion irradiation in Fe90Cr10 alloy. Nuclear Materials and Energy. 2016;**9**:476-479

[19] Mous DJW et al. Performance and applications of the first HVE 5MV Tandetron™ at the University of Madrid. AIP Conference Proceedings. 2003;**680**(1):999-1002

[20] Ishikawa J. Negative-ion source applications (invited). Review of Scientific Instruments. 2008;**79**(2):02C506

[21] Alton GD. High-intensity, heavy negative ion sources based on the sputter principle (invited). Review of Scientific Instruments. 1994;**65**(4):1141-1147

[22] High Voltage Engneering Europa B.V, Manual 5.0 MV Tandetron accelerator A-4-35-XXX-0001. 2001

[23] Tesmer JR, Nastasi MA. Handbook of modern ion beam materials analysis. In: MRS Symposium Proceedings Series. Materials Research Society; 1995

[24] Pascual Izarra C. Experimental determination of stopping forces for ions in matter. In: Física Aplicada. Universidad Autónoma de Madrid; 2004

[25] Hinterberger F. CERN Accelerator School: Small Accelerators. EAC; 2006

[26] Greinacher H. Über eine methode, Wechselstrom mittels elektrischer Ventile und Kondensatoren in hochgespannten Gleichstrom umzuwandeln. Zeitschrift für Physik. 1921;**4**(2):195-205

[27] Stodel C et al. Targets for S3 at SPIRAL2. Nuclear Instruments and Methods in Physics Research Section A: Accelerators, Spectrometers, Detectors and Associated Equipment. 2010;**613**(3):480-485

[28] Ziegler JF, Ziegler MD, Biersack JP. SRIM – The stopping and range of ions in matter. Nuclear Instruments and Methods in Physics Research Section B: Beam Interactions with Materials and Atoms. 2010;**268**(11-12):1818-1823

[29] Roldán M et al. The effect of triple ion beam irradiation on cavity formation on pure EFDA iron. Journal of Nuclear Materials. 2016;**479**:100-111

[30] Beck L et al. Ion irradiation and radiation effect characterization at the JANNUS-Saclay triple beam facility. Journal of Materials Research. 2015;**30**(09):1183-1194

[31] García-Cortés I et al. Study of damage in binary Fe85Cr15 alloys irradiated by ions and the effect of an external magnetic field during irradiation. Journal of Nuclear Materials. 2019;**517**:138-147

[32] Gigax JG et al. The influence of ion beam rastering on the swelling of self-ion irradiated pure iron at 450°C. Journal of Nuclear Materials. 2015;**465**:343-348

[33] Getto E et al. Effect of irradiation mode on the microstructure of self-ion irradiated ferritic-martensitic alloys. Journal of Nuclear Materials. 2015;**465**:116-126

[34] Robinson MT, Torrens IM. Computer simulation of atomic-displacement cascades in solids in the binary-collision approximation. Physical Review B. 1974;**9**(12):5008-5024

[35] Robinson MT. Slowing-down time of energetic atoms in solids. Physical Review B. 1989;**40**(16):10717-10726

[36] Roldán M et al. Effect of helium implantation on mechanical properties of EUROFER97 evaluated by nanoindentation. Journal of Nuclear Materials. 2014;**448**(1-3):301-309

[37] Skuratov VA et al. Swift heavy ion tracks in $Y_2Ti_2O_7$ nanoparticles in EP450 ODS steel. Journal of Nuclear Materials. 2015;**456**:111-114

[38] Skuratov VA et al. Radiation stability of the ODS alloys against swift heavy ion impact. Journal of Nuclear Materials. 2013;**442**(1-3):449-457

[39] Kaoumi D, Adamson J, Kirk M. Microstructure evolution of two model

ferritic/martensitic steels under in situ ion irradiation at low doses (0-2 dpa). Journal of Nuclear Materials. 2014;**445**(1-3):12-19

[40] Jenkins ML. Characterisation of radiation-damage microstructures by TEM. Journal of Nuclear Materials. 1994;**216**:124-156

[41] Jenkins ML, Kirk MA. Characterization of Radiation Damage by TEM. Institute of Physics; 2001

[42] Race C. The Modelling of Radiation Damage in Metals Using Ehrenfest Dynamics. Berlin Heidelberg: Springer Theses; 2010. ISBN 978-3-642-15439-3

[43] Zhang L et al. Properties of He clustering in α-Fe grain boundaries. Journal of Nuclear Materials. 2015;**459**:247-258

[44] Gai X et al. Helium bubbles in bcc Fe and their interactions with irradiation. Journal of Nuclear Materials. 2015;**462**:382-390

[45] Morishita K, Sugano R, Wirth BD. MD and KMC modeling of the growth and shrinkage mechanisms of helium-vacancy clusters in Fe. Journal of Nuclear Materials. 2003;**323**(2-3):243-250

[46] Caturla MJ, Ortiz CJ, Fu CC. Helium and point defect accumulation: (ii) Kinetic modelling. Comptes Rendus Physique. 2008;**9**(3-4):401-408

[47] Dethloff C. Modeling of Helium Bubble Nucleation and Growth in Neutron Irradiated RAFM Steels. KIT scientific publishing; 2012. ISBN 978-3-86644-901-5

[48] Dethloff C et al. Modeling of helium bubble nucleation and growth in neutron irradiated boron doped RAFM steels. Journal of Nuclear Materials. 2012;**426**(1-3):287-297